Journal of Applied Physics

RESEARCH ARTICLE | AUGUST 11 2025

Structural and electronic properties of transferred graphene on yttrium iron garnet (111)

Thang Dinh Phan ; Shunsuke Tsuda; Riku Goto; Naoka Nagamura ; Ovidiu Cretu ; Koji Kimoto ; Koichiro Yaji

J. Appl. Phys. 138, 064301 (2025)
https://doi.org/10.1063/5.0283562

AIP Publishing

Journal of Applied Physics ARTICLE pubs.aip.org/aip/jap

Structural and electronic properties of transferred graphene on yttrium iron garnet (111)

Cite as: J. Appl. Phys. 138, 064301 (2025); doi: 10.1063/5.0283562
Submitted: 2 June 2025 · Accepted: 19 July 2025 ·
Published Online: 11 August 2025

Thang Dinh Phan,[1] Shunsuke Tsuda,[1] Riku Goto,[1,2] Naoka Nagamura,[1,2] Ovidiu Cretu,[1] Koji Kimoto,[1] and Koichiro Yaji[1,3,a)]

AFFILIATIONS

[1]Center for Basic Research on Materials, National Institute for Materials Science, Tsukuba 305-0003, Japan
[2]Faculty of Advanced Engineering, Tokyo University of Science, Katsushika, Tokyo
[3]Unprecedented-scale Data Analytics Center, Tohoku University, Sendai 980-8578, Japan

[a)]**Author to whom correspondence should be addressed:** yaji.koichiro@nims.go.jp

ABSTRACT

Graphene fabricated on magnetic insulators holds great potential for developing novel functional materials and applications in spintronics devices. In the present study, we have investigated the structural and electronic properties of transferred single-layer graphene (SLG) on the yttrium iron garnet (111) [YIG(111)] substrate. Here, spin polarization in SLG/YIG(111) is reported in the previous study. Our angle-resolved photoemission spectroscopy visualizes the electronic band structure of SLG/YIG(111) and demonstrates an intact Dirac band with *p*-type doping in SLG/YIG(111). Therefore, based on a collaborative consideration of the previous and present studies, we conclude that the spin-polarized Dirac electrons exist in SLG/YIG(111).

I. INTRODUCTION

Graphene exhibits remarkable characteristics, including extraordinary mechanical properties,[1] excellent electronic transport,[2–5] long spin diffusion lengths,[6–12] significant quantum phenomena such as the quantum Hall effect (QHE),[13–19] and the quantum spin Hall effect (QSHE).[6,19–26] These characteristics make graphene an ideal material for developing next-generation spintronics devices. One of the key goals in designing graphene spintronics devices is to induce and control spin polarization in the conducting electrons. The electronic state of pure graphene is inherently non-magnetic. This property can be modified with doping, such as mixing graphene with magnetic nanoparticles,[26–28] synthesizing magnetic materials on graphene,[29,30] or modifying them with covalent bonds.[31,32] However, the doping processes can affect the specific electronic properties of graphene. One of the challenges is to induce spin polarization in graphene while maintaining the Dirac electronic state.

Graphene grown on an yttrium iron garnet (YIG) substrate has attracted much attention because its unique electronic transport properties are preserved even under magnetic proximity effects, without introducing unwanted disturbances to the graphene lattice or charge transport characteristics.[33–36] Here, the YIG is a magnetic insulator capable of inducing spin alignment in adjacent conductive layers while remaining electrically insulating. Accordingly, graphene/YIG heterostructures are regarded as promising platforms for inducing spin polarization in graphene via magnetic proximity effects, without relying on direct spin injection. This nonchemical spin interaction enables the preservation of graphene's intrinsic band structure, in contrast to direct coupling with ferromagnetic metals, which often modifies the band structure and degrades its electronic performance. As a result, graphene/YIG heterostructures provide a viable route for realizing graphene-based spintronic devices, including spin field-effect transistors (FETs). Remarkably, a significant spin asymmetry (>10%) is demonstrated in the SLG/YIG heterostructure at the Fermi level (E_F).[37] We note here that it is important to verify whether the Dirac band is modified by the interaction between graphene and the substrate. However, the study of the spin polarization in Ref. 37 employed a wave-number-integrated technique. Thus, the band structure, essential to understanding the functions of the materials, has yet to be clarified.

The electronic band structure of graphene can be explained by the tight-binding model.[38,39] Angle-resolved photoemission spectroscopy (ARPES) offers experimental visualization of the band structure of graphene. The electronic structure of graphene consists of two electron bands originating from σ and π bonds. The π electrons form a Dirac band with linear dispersion, and the valence and conduction bands cross at the K point in the Brillouin zone (BZ); this crossing point is known as the Dirac point. In free-standing graphene, the charge-neutral point is located at the E_F. On the other hand, when a substrate exists, electrons or holes are doped from the substrate into the graphene due to charge transfer, thereby modifying the energy of the charge-neutral point. In other words, the electronic state and the electrical conductivity of graphene can be controlled by tuning the doping. Carrier doping into the graphene's Dirac band is crucial for designing devices based on band engineering because the novel transport properties above are derived from the linear dispersion of the electrons at E_F. For example, in graphene on a SiC(0001) substrate,[40,41] the Dirac band shifts to the higher binding energy side due to electron transfer, resulting in *n*-type Dirac carriers. It has been reported that the Dirac band with *p*-type doping is realized by the adsorption of O_2/water molecules on graphene on SiO_2/Si.[42,43] In this case, the linear dispersion is maintained. There are also cases, such as graphene on Au-doped SiC (0001) and graphene on Bi-doped Ir(111), where the linear dispersion is broken and the bandgap opens at the Dirac point.[44,45]

In the present study, we have investigated the structural and electronic properties of SLG transferred onto YIG(111) [SLG/YIG (111)] using micro-Raman spectroscopy, transmission electron microscopy (TEM), and ARPES. TEM measurements show that our SLG has a multi-domain structure. The ARPES measurements visualize the band structure of SLG/YIG. We demonstrate that the intact Dirac band exists on the YIG(111) substrate. We also show that the energy of the Dirac point is located above the E_F, meaning that the Dirac band is doped with *p*-type.

II. EXPERIMENTAL METHODS

We used commercially available SLG manufactured by Graphenea, Inc. The SLG was transferred onto the surface of the YIG thin film, as described elsewhere.[46,47] We used a commercial YIG(111) thin film, which was epitaxially grown on a gadolinium gallium garnet (GGG) single crystal.

Micro-Raman spectroscopy was utilized to characterize graphene in the SLG/YIG(111) heterostructure. In the Raman measurements, we used a green laser with a wavelength of 532 nm. The scanning range was conducted in a wide frequency range, from ∼100 to ∼3000 cm^{-1}, to ensure that the full range, including the Raman spectra of the YIG, was observed. The measurements were performed at room temperature.

In the TEM experiments, we aim to confirm the quality of the commercial SLG. The samples for TEM were different from those for ARPES, but they were obtained from the same batch. A free-standing SLG was initially transferred to a lacey carbon TEM grid made of molybdenum. Following the transfer, the sample was annealed at 450 °C in a high-vacuum chamber for 2 h. The clean, annealed sample was then placed on the stage of the TEM, where experiments were conducted using a Thermo Fisher Scientific Titan operated at an acceleration voltage of 80 kV in scanning transmission electron microscopy (STEM) mode, with a probe current of ∼30 pA. The experiments were carried out using two observation modes: (i) high-resolution TEM operation with a beam convergence of approximately 20 mrad, which provides a standard TEM image, and (ii) diffraction mapping with a beam convergence of about 1 mrad, which yields the orientation map of the free-standing graphene.

The photoemission electron microscopy (PEEM) and ARPES measurements were conducted at the National Institute for Materials Science (NIMS).[47,48] For the PEEM measurements, the mercury lamp with a photon energy of 5.2 eV was used as the excitation light source. The helium discharge lamp with a photon energy of 21.2 eV (He I) was used for ARPES. The base pressure of the analysis chamber is maintained at approximately 1.5×10^{-8} Pa. The sample temperature was set to 40 K for both measurements.

III. RESULTS AND DISCUSSION

Raman spectroscopy is helpful in identifying the number of layers in graphene films due to its unique Raman signals, specifically the G band and the 2D band. The G band results from the in-plane vibrations of sp^2-bonded carbon atoms. In contrast, the 2D band arises from a two-phonon process that involves two intervalleys scattering between the equivalent high-symmetry points, *K* and *K′*, in a BZ.[49–51] The 2D band intensity significantly depends on the number of graphene layers. Therefore, we can assess the number of graphene layers by analyzing the intensity ratio between the 2D band and the G band.[52]

Figure 1(a) shows an optical image of SLG/YIG(111), in which we can recognize that the sample surface is almost homogeneous. Figure 1(b) is a Raman mapping of the 2D peak intensity of the graphene over a $50 \times 30\,\mu m^2$ area. The mapping was performed from a 2D peak area with starting and finishing points at 1640 and 1712 cm^{-1}, respectively. The background of the mapping is removed using the vector transformation penalized spline (VTPspline) method.[53] The Raman spectra taken at #1–#3 are exhibited in Fig. 1(c). The Raman spectrum in #1 is predominantly contributed by peaks in the region of 100–1500 cm^{-1}, which are Raman scattering of YIG as detailed in Refs. 54 and 55, while the peak at ∼1580 cm^{-1} (G band) and ∼2700 cm^{-1} (2D band) of graphene is not observed. On the other hand, the G and 2D bands appear in #2 and #3. In #2, the G (2D) band with a center peak at ∼1581 cm^{-1} (∼2675 cm^{-1}) appears. For the Raman spectrum in #3, we find the G and 2D bands at ∼1579 and ∼2693 cm^{-1}, respectively.

We here mention three reasons why area #2 in Fig. 1(b) corresponds to SLG. The first reason is the intensity ratio between the 2D band and the G band. In the case of SLG, the intensity of the 2D band is substantially higher than that of the G band, where the intensity ratio is more than 2.[56–58] In Fig. 1(c), the Raman spectrum observed in #2 shows an intensity ratio of around 2.4. On the other hand, in the Raman spectra taken in #3, the intensity ratio is 1.3. This indicates that the gray areas in Fig. 1(b), including region #2, represent SLG, while the white areas, including region #3, represent multilayer graphene. The second reason is based on the

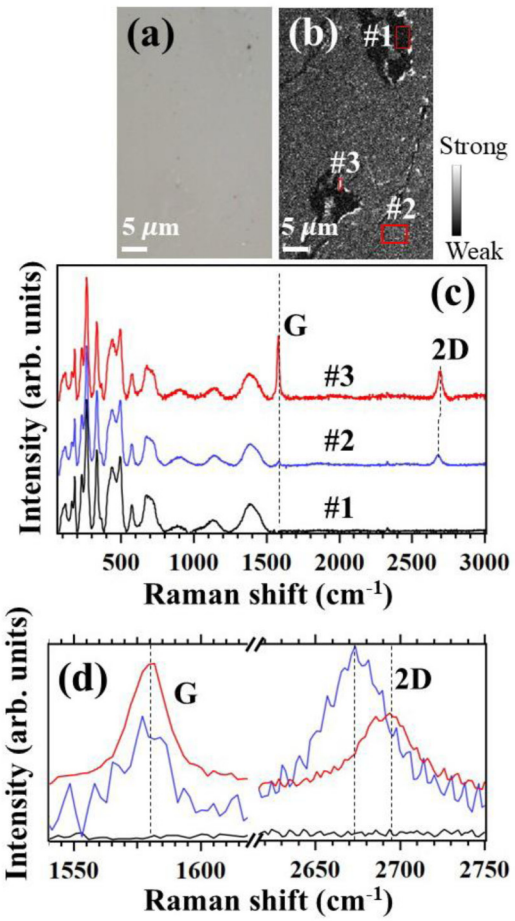

FIG. 1. (a) Optical image and (b) Raman mapping of the 2D peak intensity of the graphene over a 50 × 30 μm^2 area of SLG/YIG(111). (c) Raman spectra obtained from #1 to #3 in (b). (d) The G and 2D band regions expanded from (c).

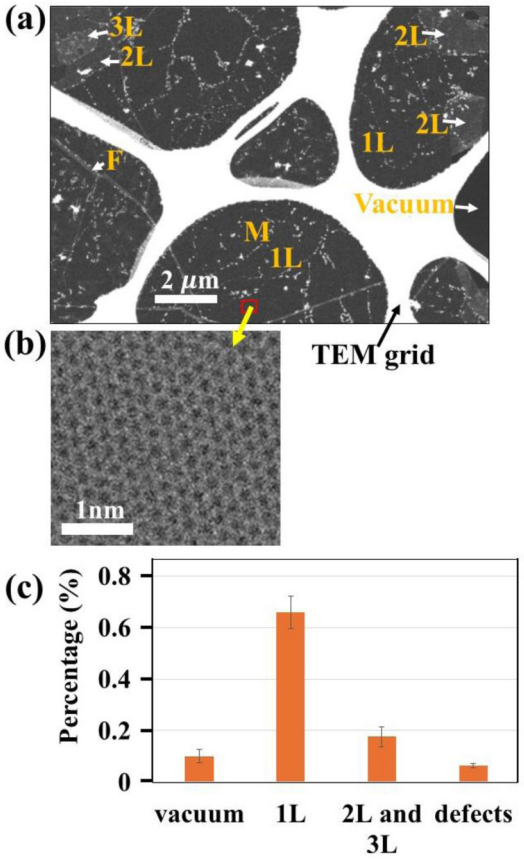

FIG. 2. (a) TEM image of our SLG. The labels "1L," "2L," and "3L" correspond to one, two, and three layers of graphene, respectively. The labels "F" and "M" refer to folds in the graphene film and metal particles, respectively. (b) Atomic resolution image of the rectangular region in (a). (c) Histogram of the number of layers of graphene.

wavenumber position of the 2D band in relation to the incident photon energy. For single-layer graphene, the peak center of the 2D band is approximately 2685 cm^{-1} for a laser wavelength of 514 nm and about 2640 cm^{-1} for a wavelength of 633 nm, as shown in a previous study.[50] In our case, we utilize a laser wavelength of 532 nm. Therefore, the peak center of the 2D band (2675 cm^{-1}) for single-layer graphene should appear in the range of 2640–2685 cm^{-1}, which well explains the experimental results. The significant shift of the 2D peak at approximately 18 cm^{-1} is an important change, which is the third reason. This is consistent with the assumption that they correspond to SLG and multilayer graphene.[50]

Figure 2(a) shows a TEM image of SLG from the same batch as SLG used to transfer onto YIG(111). In the image, the gray areas represent the suspended SLG, and the intensity of the contrast color indicates the number of graphene layers. The white structures represent the amorphous carbon mesh used to support the SLG on the TEM grid. The darkest area on the left side indicates the holding section without graphene. The atomic resolution image in Fig. 2(b) demonstrates the high quality of our sample.

Figure 2(c) presents a histogram illustrating the distribution of single-layer, bilayer, and trilayer regions, along with defects such as folds and metal particles, as identified in Fig. 2(a). The histogram indicates that the SLG region occupies a significant portion of the area, comprising approximately 70%. In comparison, bilayer and trilayer graphene account for 20% of the area. The TEM results serve as a third reason, alongside the two reasons mentioned above, supporting the conclusion that our graphene transferred onto the YIG substrate is predominantly a homogeneous single layer. Therefore, the thickness of the graphene sheet is estimated to be approximately 0.345 nm, which is consistent with Ref. 46.

Figures 3(a) and 3(b) show the PEEM and ARPES intensity mapping at the constant binding energy of 0.2 eV, respectively. The PEEM measurements are performed with a 48 μm field of view (FoV), as shown in Fig. 3(a). The white spots can be contaminants,

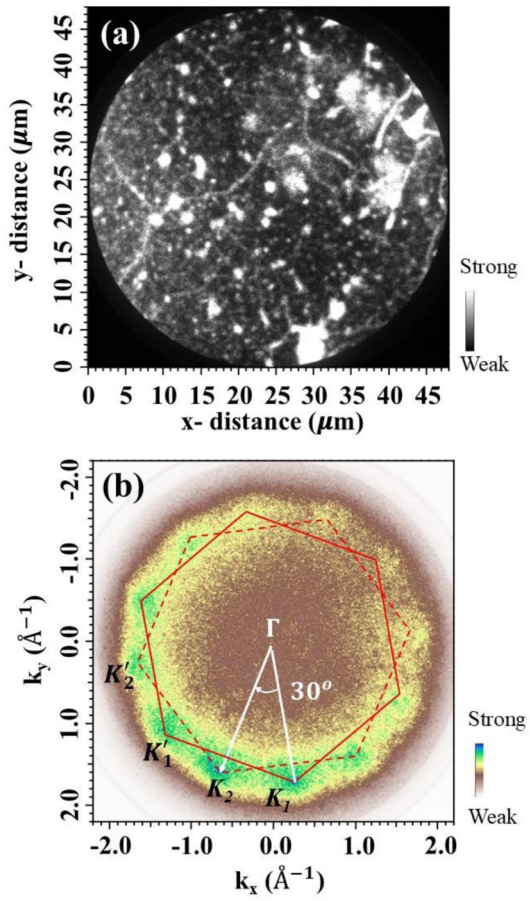

FIG. 3. (a) PEEM image of SLG/YIG(111). (b) Constant energy ARPES intensity mapping at the binding energy of 0.2 eV.

such as residual polymethyl methacrylate (PMMA) from the sample preparation process. The ARPES measurements were carried out in this FoV. Figure 3(b) shows the constant energy ARPES intensity mapping at the binding energy of 0.2 eV with the FoV of 5.01 Å^{-1}. We find 12 prominent ARPES intensities where the angles between adjacent ones are ∼30°. In addition, there are weak ARPES signals between these main intensities. This suggests that our sample has a multi-domain structure in which the 30° rotated domain is the majority, but the minor domains are producing weaker ARPES signals. Our sample is a commercial graphene sheet attributed to being grown on polycrystalline copper foil using the CVD technique and then transferred onto the YIG(111)/GGG substrate. During the CVD process, carbon atoms from the gas source (such as CH_4) can initiate the growth of graphene at various points on the copper surface, resulting in extremely small graphene islands. Since graphene islands grow on different crystallographic orientations of copper grains, their aligned lattices with their respective underlying copper grains will have a rotational mismatch when they merge. This generates a complex rotational disorder in CVD-grown graphene sheets.[59,60] The rotational mismatch of graphene grains can reduce the mobility of graphene electrons, leading to multiple Dirac bands and broadening the band structure.[61]

A double broadened Dirac band of CVD-grown graphene can be observed in ARPES mapping due to the two orientational domain groups rotated by a maximum angle of 30° with respect to each other, as demonstrated by Dabrowski *et al.*[62] The broadening of the observed Dirac band originates from the tiny orientational domains. In our case, graphene is grown using the CVD technique and then transferred onto the YIG substrate. The bilayer and trilayer graphene identified in Fig. 2(a) also contributed to the ARPES signal of the graphene on YIG(111).[63] Using four-dimensional transmission electron microscopy (4D-STEM) (Fig. S1 in the supplementary material), we confirmed that the graphene sheet comprises numerous grains. Therefore, the ARPES result shown in Fig. 3(b) is reasonable compared with the 4D-STEM results.

Figure 4(a) shows the ARPES intensity of SLG/YIG(111) taken along the $\overline{\Gamma K}$ direction. The Dirac band in the first BZ side is observed due to the interference effect in the photoelectron emission process. In graphene/graphite, the photoemission intensity is combined by photoelectrons from A and B atoms in a unit cell. The ARPES intensity in the first BZ results from positive interference between the photoelectrons from the A and B atom groups, known as the Brillouin-zone-selection effect.[64,65] We note that no bands derived from the YIG(111) substrate are observed near the E_F because the YIG(111) is a ferromagnetic insulator with a moderate gap (2.8 eV).[66] The momentum distribution curves (MDCs) are displayed in Fig. 4(b). Figure 4(c) expresses the peak positions obtained from the MDCs. We find that the Dirac band of SLG/YIG (111) crosses the E_F at 1.65 Å^{-1}. This indicates that the Dirac point is located above the Fermi level. As a reference, we show the peak position of MDCs of the SLG/SiC data, which is backfolded at 0.4 eV, indicating that the Dirac point is below the E_F.

In the previous study, it was demonstrated that spin polarization is induced in the valence band near the E_F in SLG/YIG(111) using spin-polarized metastable He atom deexcitation spectroscopy.[37] This experimental technique is extremely surface-sensitive; hence, the authors conclude that the Dirac electrons in graphene are spin-polarized. However, the existence of the Dirac band in graphene on the YIG(111) substrate is unclear because metastable helium scattering is a wave-number-integrated technique. Thus, one cannot rule out the possibility that the Dirac band has been modified due to the interaction between graphene and the YIG substrate. In addition, the existence of the electronic state derived from the YIG(111) substrate near the Fermi level is also not mentioned. To clarify this outstanding issue, the present study visualizes the band structure of SLG/YIG(111) using ARPES and demonstrates that an intact Dirac band exists in SLG/YIG(111). On the other hand, SLG on the YIG(111) substrate gives rise to the exchange interaction between the π electrons in graphene and the nearby spin-polarized 3d electrons of Fe in the YIG(111).[34,37,67] Based on the collaborative consideration of the previous and present studies, we conclude that spin-polarized Dirac electrons exist in SLG/YIG(111).

In ideal free-standing graphene, the charge-neutral point, corresponding to the Dirac point, is located at the E_F.[5,38,68] In previous

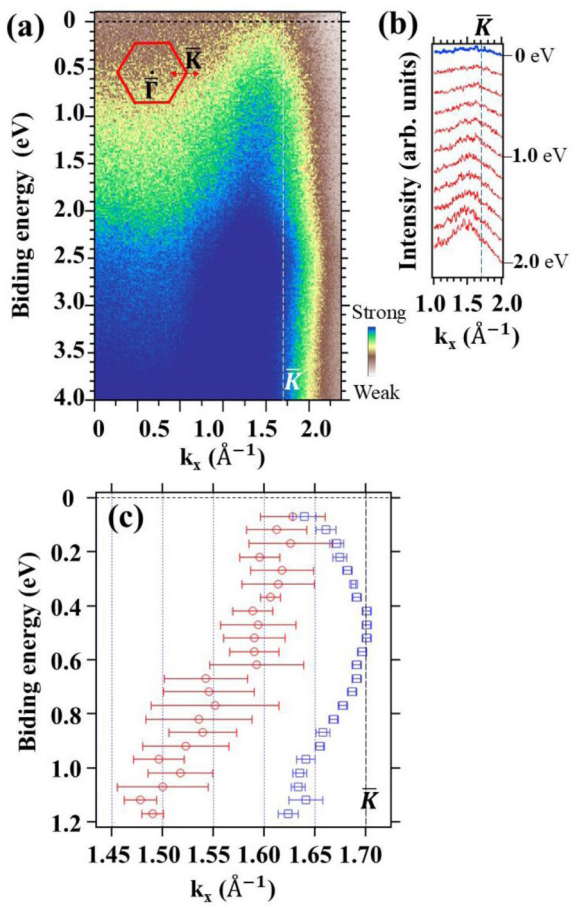

FIG. 4. (a) The ARPES intensity of SLG/YIG(111) along $\bar{\Gamma}\bar{K}$. (b) MDCs obtained from the ARPES intensity shown in (a). The energy range of 0.0–2.0 eV with an energy step of 0.1 eV is examined. (c) Peak position plots (circles) obtained from MDCs shown in (b). The square was obtained as a reference from ARPES measurements of SLG/SiC(0001) (Fig. S2 in the Supplementary material).

studies, the Dirac cone of graphene reaches a lower position than the E_F, such as SLG on Ni(111), Co(0001),[69] and SiC(0001),[70,71] the electrons of the substrate material will transport to the graphene, resulting in an n-type doping. On the other hand, we demonstrate the *p*-type-doped Dirac band in SLG/YIG(111). The p-type property of SLG/YIG(111) can be caused by the YIG substrate itself being *p*-type.[72] The *p*-type doping in graphene introduces the following advantages: (i) Improved hole control, allowing more hole carriers to transfer to graphene FETs.[73] (ii) Facilitate the creation of *p-n* junctions in graphene-based devices, which are essential for diodes, transistors, and photovoltaic applications, enhancing power efficiency.[74,75] (iii) Enhanced opto-electronic performance: The *p*-type doping can enhance graphene's optical absorption or emission characteristics, making it suitable for photodetectors and light-emitting devices, and can improve charge separation and transport, boosting device efficiency.[74] (iv) Enhancing stability and work function by aligning graphene's work function with materials that require high-work-function electrodes, such as hole-injection layers in organic light-emitting diodes or organic photovoltaics.[77,78] (v) The *p*-type doping can make graphene less reactive to certain environmental factors, enhancing the stability of devices.[78] (vi) Tailored bandgap engineering: The *p*-type doping can assist in opening or modulating graphene's bandgap, enabling its use in semiconductor-like applications.[79,80]

IV. CONCLUSION

We have investigated the structural and electronic properties of SLG/YIG(111) by micro-Raman spectroscopy, TEM, and ARPES. The 12 prominent ARPES intensities were found from the Fermi surface mapping, indicating that the major domains are rotated 30° relative to each other. In SLG/YIG(111), we have demonstrated that the Dirac band exhibits linear dispersion. In the previous paper, spin polarization was observed in the valence band near the Fermi level.[37] Therefore, we have concluded that the spin-polarized Dirac electrons exist in SLG/YIG(111). Furthermore, the Dirac band is doped in the *p*-type in SLG/YIG(111). The SLG/YIG (111) can be a promising material for spintronics applications.

SUPPLEMENTARY MATERIAL

See the supplementary material for the results of 4D-STEM and ARPES for SLG on SiC(0001).

ACKNOWLEDGMENTS

The authors thank Fumiya Arai for their technical support in ARPES measurements. The present work is financially supported by the Japan Society for the Promotion of Science KAKENHI (Grant Nos. JP21K04633, JP22H05145, JP24K01352, and JP24K08253); the Innovative Science and Technology Initiative for Security under Grant No. JPJ004596; ATLA, Japan; Iketani Science and Technology Foundation; and the JST, CREST, Japan under Grant No. JPMJCR2435.

AUTHOR DECLARATIONS

Conflict of Interest

The authors have no conflicts to disclose.

Author Contributions

Thang Dinh Phan: Formal analysis (lead); Investigation (lead); Visualization (lead); Writing – original draft (lead). **Shunsuke Tsuda:** Investigation (supporting); Validation (supporting); Writing – review & editing (supporting). **Riku Goto:** Investigation (supporting). **Naoka Nagamura:** Investigation (supporting). **Ovidiu Cretu:** Formal analysis (supporting); Investigation (supporting). **Koji Kimoto:** Formal analysis (supporting); Investigation (supporting). **Koichiro Yaji:** Conceptualization (lead); Funding acquisition (lead); Resources (lead); Supervision (lead); Validation (lead); Writing – review & editing (lead).

DATA AVAILABILITY

The data that support the findings of this study are available from the corresponding author upon reasonable request.

REFERENCES

[1]C. Gómez-Navarro, M. Burghard, and K. Kern, Nano Lett. **8**(7), 2045–2049 (2008).
[2]K. S. Novoselov, A. K. Geim, S. V. Morozov, D. Jiang, M. I. Katsnelson, I. V. Grigorieva, S. V. Dubonos, and A. A. Firsov, Nature **438**, 197–200 (2005).
[3]S. Das Sarma, S. Adam, E. H. Hwang, and E. Rossi, Rev. Mod. Phys. **83**, 407 (2011).
[4]Y. S. Dedkov and M. Fonin, New J. Phys. **12**, 125004 (2010).
[5]A. H. Castro Neto, F. Guinea, N. M. R. Peres, K. S. Novoselov, and A. K. Geim, Rev. Mod. Phys. **81**, 109 (2009).
[6]N. Tombros, C. Jozsa, M. Popinciuc, H. T. Jonkman, and B. J. van Wees, Nature **448**, 571–574 (2007).
[7]M. Popinciuc, C. Józsa, P. J. Zomer, N. Tombros, A. Veligura, H. T. Jonkman, and B. J. van Wees, Phys. Rev. B **80**, 214427 (2009).
[8]B. Dlubak, P. Seneor, A. Anane, C. Barraud, C. Deranlot, D. Deneuve, B. Servet, R. Mattana, F. Petroff, and A. Fert, Appl. Phys. Lett. **97**, 092502 (2010).
[9]W. Han and R. K. Kawakami, Phys. Rev. Lett. **107**, 047207 (2011).
[10]T. Y. Yang, J. Balakrishnan, F. Volmer, A. Avsar, M. Jaiswal, J. Samm, S. R. Ali, A. Pachoud, M. Zeng, M. Popinciuc, G. Güntherodt, B. Beschoten, and B. Özyilmaz, Phys. Rev. Lett. **107**, 047206 (2011).
[11]T. Maassen, J. Jasper van den Berg, N. Ijbema, F. Fromm, T. Seyller, R. Yakimova, and B. J. van Wees, Nano Lett. **12**, 1498–1502 (2012).
[12]B. Dlubak, M. Martin, C. Deranlot, B. Servet, S. Xavier, R. Mattana, M. Sprinkle, C. Berger, W. A. De Heer, F. Petroff, A. Anane, P. Seneor, and A. Fert, Nat. Phys. **8**(7), 557–561 (2012).
[13]Z. Jiang, Y. Zhang, Y. W. Tan, H. L. Stormer, and P. Kim, Solid State Commun. **143**, 14–19 (2007).
[14]M. O. Goerbig, C. R. Phys. **12**(4), 369–378 (2011).
[15]K. S. Novoselov, Z. Zhang, S. V. Morozov, H. L. Stormer, U. Zeitler, J. C. Maan, G. S. Boebinger, P. Kim, and A. K. Geim, Science **315**, 1379 (2007).
[16]T. P. Cysne, J. H. Garcia, A. R. Rocha, and T. G. Rappoport, Phys. Rev. B **97**, 085413 (2018).
[17]Y. Wang, X. Gao, K. Yang, P. Gu, X. Lu, S. Zhang, Y. Gao, N. Ren, B. Dong, Y. Jiang, K. Watanabe, T. Taniguchi, J. Kang, W. Lou, J. Mao, J. Liu, Y. Ye, Z. Han, K. Chang, J. Zhang, and Z. Zhang, Nat. Nanotechnol. **17**, 1272–1279 (2022).
[18]Y. Zhang, Y. W. Tan, H. L. Stormer, and P. Kim, Nature **438**, 201–204 (2005).
[19]Z. Li, Z. Gao, J. Hu, C. Mattioli, P. Ding, W. Xu, Y. Sun, J. Li, D. Zhong, Y. Huang, G. Li, F. Song, A. Gourdon, L. N. Kantorovich, F. Besenbacher, and M. Yu, Cell Rep. Phys. Sci. **4**, 101492 (2023).
[20]S. Murakami, N. Nagaosa, and S.-C. Zhang, Science **301**, 1348–1351 (2003).
[21]J. Sinova, D. Culcer, Q. Niu, N. A. Sinitsyn, T. Jungwirth, and A. H. MacDonald, Phys. Rev. Lett. **92**, 126603 (2004).
[22]C. L. Kane and E. J. Mele, Phys. Rev. Lett. **95**, 226801 (2005).
[23]A. Avsar, I. J. Vera-Marun, J. Y. Tan, G. K. W. Koon, K. Watanabe, T. Taniguchi, S. Adam, and B. Özyilmaz, NPG Asia Mater. **8**, e274 (2016).
[24]W. Han, K. Pi, K. M. McCreary, Y. Li, J. J. I. Wong, A. G. Swartz, and R. K. Kawakami, Phys. Rev. Lett. **105**, 167202 (2010).
[25]Q. F. Sun, Z. T. Jiang, Y. Yu, and X. C. Xie, Phys. Rev. B **84**, 214501 (2011).
[26]N. Alegret, A. Criado, and M. Prato, Curr. Med. Chem. **24**, 529–536 (2017).
[27]K. Lee, J. Lee, B. M. Jung, B. Park, and T. Kim, Appl. Surf. Sci. **478**, 733–736 (2019).
[28]S. Uten, P. Boonbanjong, Y. Prueksathaporn, K. Treerattrakoon, N. Sathirapongsasuti, N. Chanlek, S. Pinitsoontorn, P. Luksirikul, and D. Japrung, ACS Omega **9**(2), 2263–2271 (2024).
[29]D. Ağaoğulları, S. J. Madsen, B. Ögüt, A. L. Koh, and R. Sinclair, Carbon **124**, 170–179 (2017).
[30]S. Mertdinç-Ülküseven, U. Savacı, M. Lütfi Öveçoğlu, and D. Ağaoğulları, J. Mater. Res. Technol. **20**, 2558–2577 (2022).
[31]V. Georgakilas, M. Otyepka, A. B. Bourlinos, V. Chandra, N. Kim, K. Christian Kemp, P. Hobza, R. Zboril, and K. S. Kim, Chem. Rev. **112**, 6156–6214 (2012).
[32]G. L. C. Paulus, Q. H. Wang, and M. S. Strano, Acc. Chem. Res. **46**(1), 160–170 (2013).
[33]Z. Wang, C. Tang, R. Sachs, Y. Barlas, and J. Shi, Phys. Rev. Lett. **114**, 016603 (2015).
[34]J. C. Leutenantsmeyer, A. A. Kaverzin, M. Wojtaszek, and B. J. Van Wees, 2D Mater. **4**, 014001 (2017).
[35]A. Hallal, F. Ibrahim, H. Yang, S. Roche, and M. Chshiev, 2D Mater. **4**, 025074 (2017).
[36]D. A. Solis, A. Hallal, X. Waintal, and M. Chshiev, Phys. Rev. B **100**, 104402 (2019).
[37]S. Sakai, S. V. Erohin, Z. I. Popov, S. Haku, T. Watanabe, Y. Yamada, S. Entani, S. Li, P. V. Avramov, H. Naramoto, K. Ando, P. B. Sorokin, and Y. Yamauchi, Adv. Funct. Mater. **28**, 1800462 (2018).
[38]P. R. Wallace, Phys. Rev. **71**, 622–634 (1947).
[39]G. S. Painter and D. E. Ellis, Phys. Rev. B **1**, 4747–4752 (1970).
[40]H. Peng, N. B. M. Schröter, J. Yin, H. Wang, T.-F. Chung, H. Yang, S. Ekahana, Z. Liu, J. Jiang, L. Yang, T. Zhang, C. Chen, H. Ni, A. Barinov, Y. P. Chen, Z. Liu, H. Peng, and Y. Chen, Adv. Mater. **29**, 1606741 (2017).
[41]S. Ryu, L. Liu, S. Berciaud, Y.-J. Yu, H. Liu, P. Kim, G. W. Flynn, and L. E. Brus, Nano Lett. **10**, 4944–4951 (2010).
[42]D. J. Late, B. Liu, H. S. S. R. Matte, V. P. Dravid, and C. N. R. Rao, ACS Nano **6**, 5635–5641 (2012).
[43]D. J. Late, Y.-K. Huang, B. Liu, J. Acharya, S. N. Shirodkar, J. Luo, A. Yan, D. Charles, U. V. Waghmare, V. P. Dravid, and C. N. R. Rao, ACS Nano **7**, 4879–4891 (2013).
[44]D. Marchenko, A. Varykhalov, J. Sánchez-Barriga, T. Seyller, and O. Rader, Appl. Phys. Lett. **108**, 172405 (2016).
[45]I. I. Klimovskikh, M. M. Otrokov, V. Y. Voroshnin, D. Sostina, L. Petaccia, G. Di Santo, S. Thakur, E. V. Chulkov, and A. M. Shikin, ACS Nano **11**, 368 (2017).
[46]See https://www.graphenea.com/blogs/graphene-news/new-product-easy-transfer?srsltid=AfmBOorkpYUi-1QQEfL_WUx8gCsIbSneCWixDh6O4C4UbcpTmOUqf1cK for information about "Transfer graphene onto the right substrate in three easy steps: release, transfer, and removal."
[47]K. Yaji and S. Tsuda, Sci. Technol. Adv. Mater. **4**, 2328206 (2024).
[48]K. Yaji and S. Tsuda, e-J. Surf. Sci. Nanotechnol. **22**, 46–52 (2023).
[49]E. J. Heller, Y. Yang, L. Kocia, W. Chen, S. Fang, M. Borunda, and E. Kaxiras, ACS Nano **10**, 2803–2818 (2016).
[50]A. C. Ferrari, J. C. Meyer, V. Scardaci, C. Casiraghi, M. Lazzeri, F. Mauri, S. Piscanec, D. Jiang, K. S. Novoselov, S. Roth, and A. K. Geim, Phys. Rev. Lett. **97**, 187401 (2006).
[51]L. M. Malard, M. A. Pimenta, G. Dresselhaus, and M. S. Dresselhaus, Phys. Rep. **473**, 51–87 (2009).
[52]D. Graf, F. Molitor, K. Ensslin, C. Stampfer, A. Jungen, C. Hierold, and L. Wirtz, Nano Lett. **7**, 238–242 (2007).
[53]Y. Cai, C. Yang, D. Xu, and W. Gui, Anal. Methods **10**, 3525–3533 (2018).
[54]I. I. Syvorotka, D. Sugak, U. Yakhnevych, O. Buryy, D. Włodarczyk, A. Pieniążek, Y. Zhydachevskyy, N. Levintant-Zayonts, H. Savytskyy, O. Bonchyk, S. Ubizskii, and A. Suchocki, Cryst. Res. Technol. **57**, 2100180 (2022).
[55]L. Jin, K. Jia, Y. He, G. Wang, Z. Zhong, and H. Zhang, Appl. Surf. Sci. **483**, 947–952 (2019).
[56]Y. Dong, Y. Xie, C. Xu, Y. Fu, X. Fan, X. Li, L. Wang, F. Xiong, W. Guo, G. Pan, Q. Wang, F. Qian, and J. Sun, Nanotechnology **29**, 365301 (2018).
[57]E. Kim, W. G. Lee, and J. Jung, Electron. Mater. Lett. **7**, 261–264 (2011).
[58]S. Uddin and Y. W. Song, Appl. Sci. **11**, 2768 (2021).
[59]F. Pizzocchero, B. S. Jessen, L. Gammelgaard, A. Andryieuski, P. R. Whelan, A. Shivayogimath, J. M. Caridad, J. Kling, N. Petrone, P. T. Tang, R. Malureanu,

J. Hone, T. J. Booth, A. Lavrinenko, and P. Bøggild, ACS Omega **7**, 22626–22632 (2022).
[60]H. C. Hong, J. I. Ryu, and H. C. Lee, Nanomaterials **13**, 2217 (2023).
[61]L. I. Johansson, R. Sarmiento, J. Avila, C. Xia, S. Lorcy, I. A. Abrikosov, M. C. Asensio, and C. Virojanadara, Sci. Rep. **4**, 4157 (2014).
[62]J. Dabrowski, G. Lippert, J. Avila, J. Baringhaus, I. Colambo, Y. S. Dedkov, F. Herziger, G. Lupina, J. Maultzsch, T. Schaffus, T. Schroeder, M. Kot, C. Tegenkamp, D. Vignaud, and M.-C. Asensio, Sci. Rep. **6**, 31639 (2016).
[63]K. Sugawara, N. Yamamura, K. Matsuda, W. Norimatsu, M. Kusunoki, T. Sato, and T. Takahashi, NPG Asia Mater. **10**, e466 (2018).
[64]E. L. Shirley, L. J. Terminello, A. Santoni, and F. J. Himpsel, Phys. Rev. B **51**, 13614 (1995).
[65]H. Daimon, S. Imada, H. Nishimoto, and S. Suga, J. Electron Spectrosc. Relat. Phenom. **76**, 487–492 (1995).
[66]J. Barker, D. Pashov, and J. Jackson, Electron. Struct. **2**, 044002 (2020).
[67]J. B. S. Mendes, O. Alves Santos, L. M. Meireles, R. G. Lacerda, L. H. Vilela-Leão, F. L. A. Machado, R. L. Rodríguez-Suárez, A. Azevedo, and S. M. Rezende, Phys. Rev. Lett. **115**, 226601 (2015).
[68]J. C. Slonczewski and P. R. Weiss, Phys. Rev. **109**, 272–279 (1958).
[69]A. Varykhalov, D. Marchenko, J. Sánchez-Barriga, M. R. Scholz, B. Verberck, B. Trauzettel, T. O. Wehling, C. Carbone, and O. Rader, Phys. Rev. X **2**, 041017 (2012).
[70]I. Razado-Colambo, J. Avila, D. Vignaud, S. Godey, X. Wallart, D. P. Woodruff, and M. C. Asensio, Sci. Rep. **8**, 10190 (2018).
[71]A. Vasudevan, V. Shvalya, A. Zidanšek, and U. Cvelbar, Front. Chem. Sci. Eng. **13**, 427–443 (2019).
[72]W.-K. Li and G.-Y. Guo, Phys. Rev. B **103**, 014439 (2021).
[73]S. Chae, G. Panomsuwan, M. A. Bratescu, K. Teshima, and N. Saito, ACS Appl. Nano Mater. **2**, 1350–1355 (2019).
[74]T. Huynh, T. D. Ngo, H. Choi, M. Choi, W. Lee, T. D. Nguyen, T. T. Tran, K. Lee, J. Y. Hwang, J. Kim, and W. J. Yoo, ACS Appl. Mater. Interfaces **16**, 3694–3702 (2024).
[75]G. Wang, M. Zhang, D. Chen, Q. Guo, X. Feng, T. Niu, X. Liu, A. Li, J. Lai, D. Sun, Z. Liao, Y. Wang, P. K. Chu, G. Ding, X. Xie, Z. Di, and X. Wang, Nat. Commun. **9**, 5168 (2018).
[76]C. Liu, Y. Xu, and Y. Y. Noh, Mater. Today **18**, 79–96 (2015).
[77]S. J. Kwon, T.-H. Han, T. Y. Ko, N. Li, Y. Kim, D. J. Kim, S.-H. Bae, Y. Yang, B. H. Hong, K. S. Kim, S. Ryu, and T.-W. Lee, Nat. Commun. **9**, 2037 (2018).
[78]A. Piazza, F. Giannazzo, G. Buscarino, G. Fisichella, A. L. Magna, F. Roccaforte, M. Cannas, F. M. Gelardi, and S. Agnello, J. Phys. Chem. C **119**, 22718–22723 (2015).
[79]H. Liu, Y. Liu, and D. Zhu, J. Mater. Chem **21**, 3335–3345 (2011).
[80]C. Liang, Y. Wang, and T. Li, Carbon **82**, 506–512 (2015).